International Journal of Remote Sensing and Earth Sciences Vol. 7: 53-72 (2010) © IReSES

ESTIMATION OF TIDAL ENERGY DISSIPATION AND DIAPYCNAL DIFFUSIVITY IN THE INDONESIAN SEAS

I Wayan Gede Astawa Karang[1,2,3], Fumihiko Nishio[1,3] And Takahiro Osawa[2]

Abstract. The Indonesian Seas separating the Indian Ocean from the West Pacific Ocean are representative regions of strong tidal mixing in the world oceans. In the present study, we first carry out numerical simulation of the barotropic tidal elevation field in the Indonesian Seas using horizontally two-dimensional primitive equation model. It is found that, to reproduce realistic tidal elevations in the Indonesian Seas, the energy lost by the incoming barotropic tides to internal waves within the Indonesian seas should be taken into account. The numerical experiments show that the model predicted tidal elevations in the Indonesian Seas best fit the observed data when we take into account the baroclinic energy conversion in the Indonesian Seas ~86.1 GW for the M_2 tidal constituent and ~134.6 GW for the major four tidal constituents (M_2, S_2, K_1, O_1). For this baroclinic energy conversion, the value of $K\rho$ averaged within the eastern area (Halmahera, Seram, Banda and Maluku Seas), the western area (Makassar and Flores Seas), and the southern area (Lombok Strait and Timor Passage) are estimated to be ~23 × 10^{-4} m^2s^{-1}, ~5 × 10^{-4} m^2s^{-1}, and ~10× 10^{-4} m^2s^{-1}, respectively. This value is about 1 order of magnitude more than assumed for the Indonesian Seas in previous ocean general circulation models. We offer this study as a warning against using diapycnal diffusivity just as a tuning parameter to reproduce large-scale phenomena.

Keywords: *Baroclinic energy conversion, barotropic tides, diapycnal diffusivity, Indonesian Seas, internal waves, tidal elevations*

1. Introduction

The Indonesian Seas are among the most significant generation regions of the internal tide in the world's oceans. The area is characterized by strong barotropic tidal currents [Hatayama, 1996] as well as prominent topographic features and 20-150 GW of M2 barotropic to baroclinic energy conversion is expected to occur [Niwa and Hibiya, 2001; Egbert and Ray, 2001; Simmons et al., 2004; Larrouy et al., 2007]. Internal tides generated by tide-topography interactions then break causing vigorous diapycnal mixing. Indeed, using an advection-diffusion model and archived data, a large diapycnal diffusivity exceeding 1 × 10-4 m2 s-1 is inferred for the Indonesian thermocline [Ffield and Gordon, 1992; Gordon, 1986].

The transformation of water mass properties taking place in the Indonesian Seas is important not only for local phenomena but also for global ocean heat and mass budgets. The Indonesian Throughflow (ITF) connects the main thermocline waters in the Pacific and Indian Oceans. The ITF transports relatively warm,

1 Center for Environmental Remote Sensing, Chiba University, Japan
2 CReSOS, Udayana University, Denpasar, Bali
3. Graduate School of Sciences, Department of Earth Sciences, Chiba University, Japan

low salinity thermocline water from the western Pacific Ocean through the multitude of the Indonesian Seas and straits, to the Indian Ocean [Gordon, 1986; Hirst and Godfrey, 1993; Miyama et al., 1995; Schiller et al., 1998]. Diapycnal mixing within the Indonesian Seas significantly alters the thermohaline stratification and the velocity profile of the ITF [Ffield and Gordon, 1992; Gordon et al., 1994]. For example, as the ITF carries North Pacific thermocline water from the Sulawesi Sea to the Makassar Strait and Flores Sea, then to the Banda Sea and Timor Sea, the salinity minimum at 300 db are greatly attenuated [Ffield and Gordon, 1992]. Water mass transformation in the Indonesian Seas then affects global ocean circulation. For example, Schiller et al. [1998] carried out a numerical experiment using an ocean general circulation model to show that temperature and salinity distributions in the Indian Ocean are subject to large diapycnal diffusivity in the Indonesian Seas [Ffield and Gordon, 1996].

Although vigorous diapycnal mixing in the Indonesian Seas is thus an important physical process, quantitative estimates of its intensity have not been carried out. The tidal energy available for mixing processes has also not yet been reliably determined [Ray et al., 2005]. Although Hatayama [2004] carried out vertically two-dimensional numerical experiments to demonstrate that breaking of large amplitude internal waves at Dewakang Sill in the southern Makassar Strait can produce large diapycnal diffusivity ~60 × 10-4 m2s-1, spatial distribution of "mixing hot spots" in the Indonesian Seas has not been clarified yet.

In the present study, we first show that, to reproduce realistic tidal elevations in the Indonesian Seas and surrounding region, the energy lost by incoming barotropic tides to internal waves within the Indonesia Seas should be taken into account. Next, the diapycnal diffusivity in the Indonesian Seas is quantitatively estimated in terms of the model predicted baroclinic energy conversion. In this study, we mainly focus on the most dominant M2 tidal constituent [Hatayama et al., 1996], although the results of numerical experiments for other major tidal constituents (K1, O1, and S2) are also discussed briefly.

2. Numerical Experiments

The model region in this study extends from 92oE to 142oE in longitudinal direction and from 20oS to 23oN in latitudinal direction (Figure 1). This covers the entire Indonesian Seas and surrounding region. The open boundaries are assumed sufficiently away from the Indonesian Seas to prevent the tidal field in the Indonesian Seas from being disturbed by the reflected waves from the open boundaries.

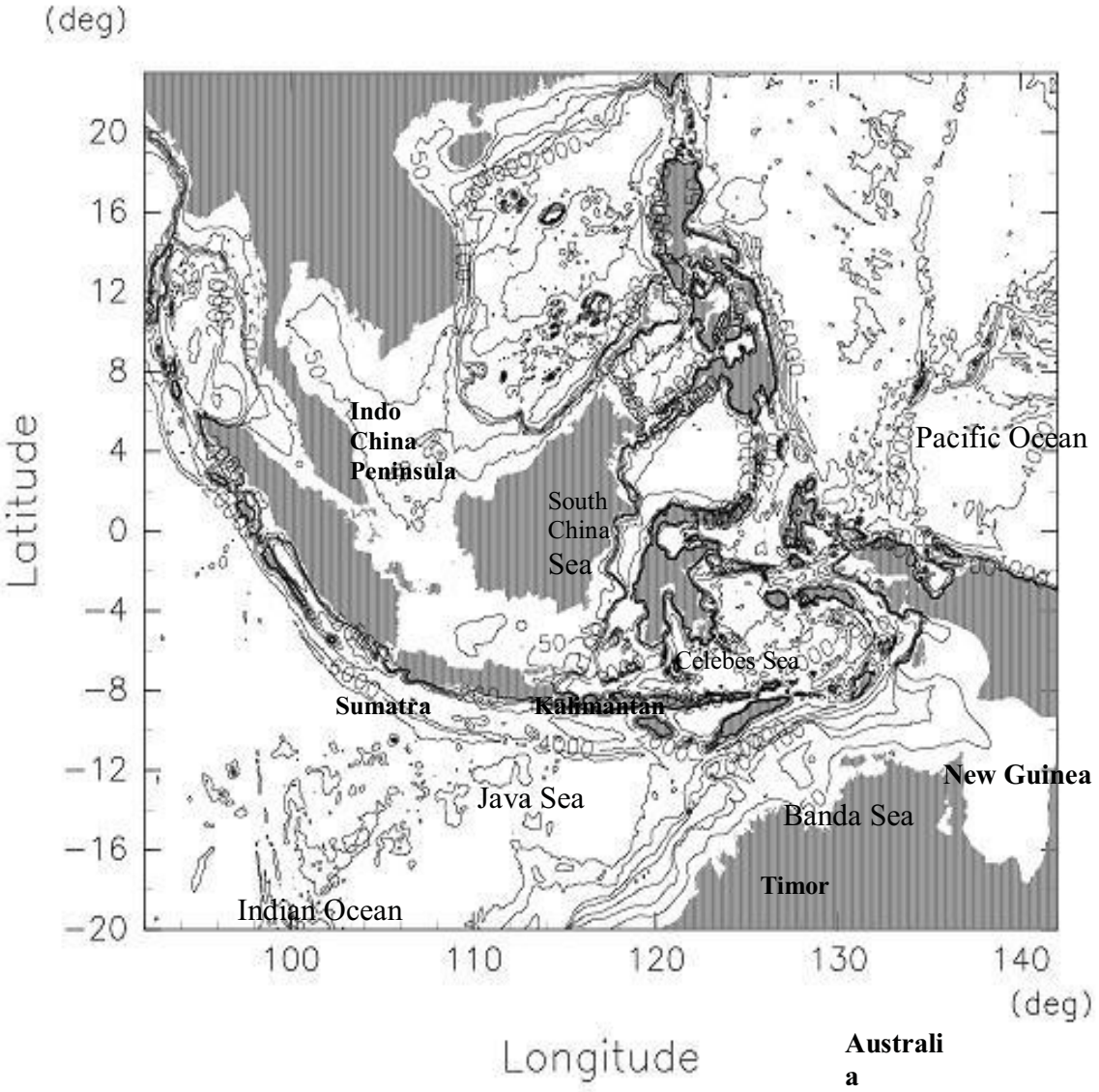

Figure 1. Model domain and bathymetry including the Indian Ocean and adjacent seas. Contours of the bathymetry are 50, 100, 200, 500, 1000, 2000, 4000, and 6000 m, respectively.

The governing equations are the horizontally two-dimensional, depth-integrated Navier-Stokes equations in Cartesians coordinate system given by

$$\frac{\partial \eta}{\partial t} + \frac{\partial}{\partial x}(uD) + \frac{\partial}{\partial y}(vD) = 0 \quad (1)$$

$$\frac{\partial}{\partial t}(uD) + \frac{\partial}{\partial x}(u^2 D) + \frac{\partial}{\partial y}(uvD) \quad fvD = gD\frac{\partial}{\partial x}(\eta - \eta_{SAL} - \beta\zeta) - C_d|\bar{\mathbf{u}}|u + F_x \quad (2)$$

$$\frac{\partial}{\partial t}(vD) + \frac{\partial}{\partial x}(uvD) + \frac{\partial}{\partial y}(v^2 D) + fuD = gD\frac{\partial}{\partial y}(\eta - \eta_{SAL} - \beta\zeta) - C_d|\bar{\mathbf{u}}|v + F_y \quad (3)$$

where t is time; x and y are defined positive eastward and northward, respectively; u and v are the depth-averaged velocities in the x and y directions, respectively; f=2 : sin φ is the Coriolis frequency with : the angular velocity of the Earth's rotation and φ latitude; g is the acceleration due to gravity; η is the free surface elevation; D=H+η with H the local ocean depth; ζ is the forcing equilibrium tide; β multiplying ζ is the effective Earth elasticity which is assumed to be 0.693 for the M_2 and 0.736 for the K_1 tidal constituent following *Kantha* [1995]; η_{SAL} is self-attraction/loading term induced by ocean tide which was calculated from the global ocean tidal model by *Matsumoto et al.* [2000]. The bottom stress is parameterized using quadratic law with a bottom drag coefficient C_d = 0.0025. F_x and F_y are horizontal viscosity terms given by

$$F_x = \frac{\partial}{\partial x}\left[2HA_H\frac{\partial u}{\partial x}\right] + \frac{\partial}{\partial y}\left[HA_H\left(\frac{\partial u}{\partial y} + \frac{\partial v}{\partial x}\right)\right] \quad (4)$$

$$F_y = \frac{\partial}{\partial y}\left[2HA_H\frac{\partial v}{\partial y}\right] + \frac{\partial}{\partial x}\left[HA_H\left(\frac{\partial u}{\partial y} + \frac{\partial v}{\partial x}\right)\right] \quad (5)$$

with A_H the horizontal eddy viscosity coefficient determined following *Smagorinsky* [1963].

The governing equations (1)-(3) are numerically solved using a finite difference method. The grid size is $(1/15)^o$ both in the longitudinal and latidunal directions. The model topography is obtained by averaging the bathymetric data from "GEBCO" within a 10 km radius at each grid point.

[10] A slip boundary condition is assumed along the land boundaries. At the open boundaries, tidal elevations are specified on the basis of the calculated results of *Matsumoto et al.* [2000]. The model is thus driven by these boundaries forcing as well as tidal potential forcing.

The model is driven for 15 days from an initial state at rest for semidiurnal and diurnal tides, by which time the model ocean attains quasistationary oscillations. The calculated time series for the final four tidal periods are harmonically analyzed to obtain the amplitude and phase of each tidal constituent. For the energy balance calculation, the data averaged over final one tidal period is used.

3. Tidal Elevation Field in the Indonesian Seas

Coamplitude and cophase charts for the M_2 tidal constituent are given in Figure 2 and 3, respectively. The spatial patterns of coamplitude and cophase charts are qualitatively consistent with those from previous numerical studies [*Hatayama et al.*, 1996; *Ray et al.*, 2005].

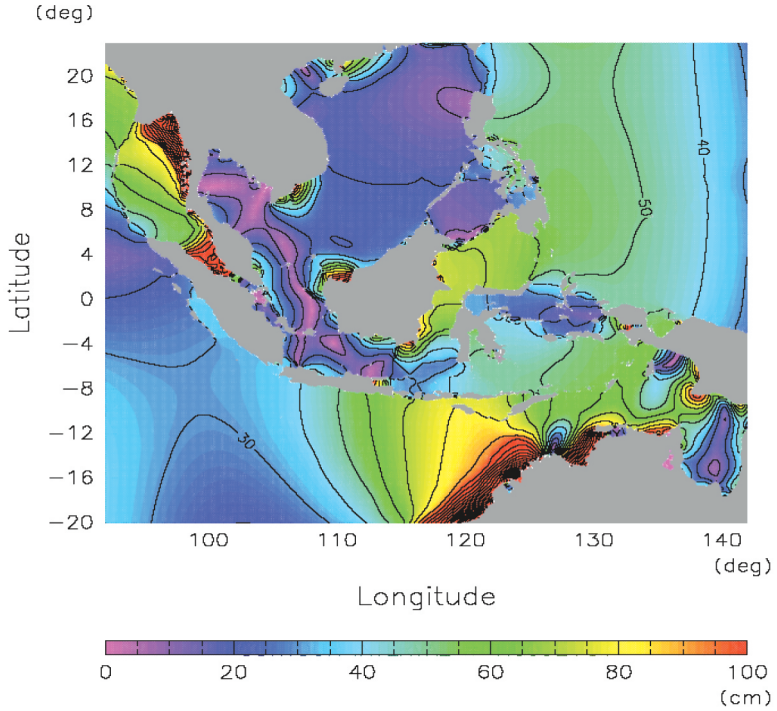

Figure 2. Calculated coamplitude chart of tidal elevations for the M_2 tide (interval is 5 cm).

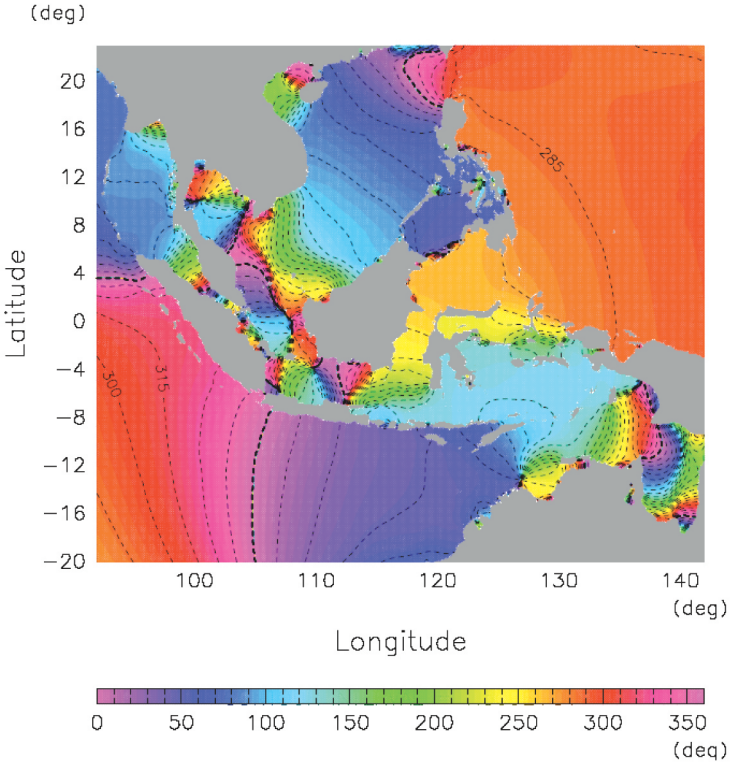

Figure 3. Calculated cophase chart of tidal elevations for the M_2 tide. The contour interval is 15 degree. The phases are referred to Greenwich.

The M_2 tide response is clearly dominated by the large tide from the Indian Ocean, where amplitudes are well over one meter off northwest Australia. This wave is delayed slightly (about 2 hours) as it passes into the Banda and Flores Seas. Those seas are sufficiently deep that high tide occurs almost simultaneously throughout both basins. From the Banda Sea, the M_2 tide passes slowly northwards through the Molucca Sea region. From the Flores Sea, it propagates slowly northwards into Makassar Strait and westwards across the Java Sea.

The calculated tidal elevations are now compared with the observed data. The observed data used here are tidal harmonic data from international coastal tide gauges records provided by *K. Matsumoto* and Department Earth and Planetary Science, University of Tokyo. Figure 4 shows the spatial distributions of the tide gauges stations in Indonesian Seas and adjacent areas. The observed data were taken from 174 coastal tide gauge stations for the major four tidal constituents (M_2, S_2, K_1, O_1). The names and locations of each station are described in appendix. We calculate the root mean-square (RMS) difference defined as

$$\mathrm{RMS} \quad \frac{1}{T}\left\{\int_0^T [\eta_{obs}\cos(\omega t-\theta_{obs})-\eta_{mod}\cos(\omega t+\theta_{mod})]^2 dt\right\}^{1/2} \qquad (6)$$

where T is the tidal period; ω is the frequency; η and θ are the amplitude and the phase, respectively; and subscripts *obs* and *mod* represent the observed and calculated harmonic constants, respectively. Figure 5 shows the RMS difference between the calculated and observed tidal elevations. The RMS difference between the models predicted tidal elevations and observed data in the Indonesian Seas averages at 11.18 cm. This value is almost the same as those of previous numerical studies (for example, the average of RMS difference of *Hatayama et al.* [1996] is 11.2 cm).

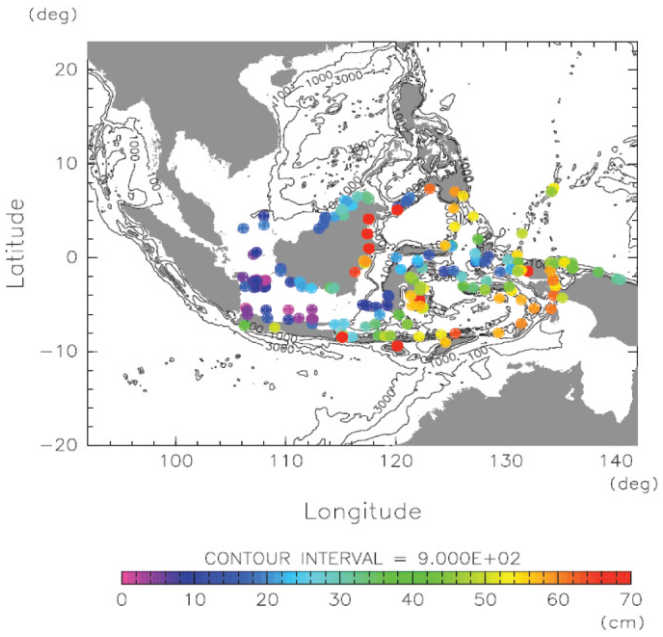

Figure 4. Spatial distribution of tides gauges station in the study area. The color scale shows the amplitude of M_2 tidal constituent for each station.

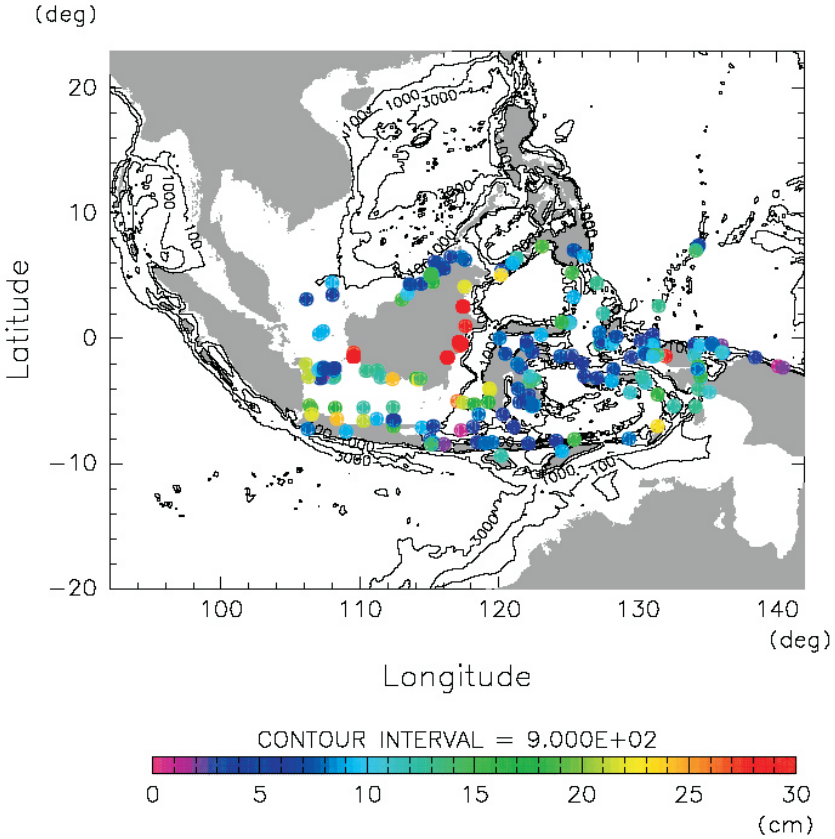

Figure 5. RMS difference between the models predicted tidal elevations and observed data.

4. Parameterization for the Baroclinic Energy Conversion

As mentioned before, large amount of incoming barotropic tidal energy is lost by the baroclinic energy conversion in the Indonesian Seas [*Niwa and Hibiya*, 2001; *Egbert and Ray*, 2001]. In order to reproduce accurate tidal elevations in the Indonesian Seas, the momentum equations (2) and (3) are modified to include the drag stress term associated with upward baroclinic energy flux in a manner similar to those of *Jayne and St. Laurent* [2001] and *Tanaka et al.* [2007].

Using a standard internal wave relationship, the upward energy flux over rough bottom topography can be expressed as

$$F_z' \cong \frac{\rho_0 (N^2 - \omega^2)^{1/2} (\omega^2 - f^2)^{1/2}}{k\omega} w^2 \quad (7)$$

where N is the buoyancy frequency; and w is the vertical velocity associated with the upward propagating internal waves with horizontal wave number k and frequency Ω [*Gill*, 1982; *St. Laurent and Garrett*, 2002]. Strictly speaking, however, this expression is valid only for small scale topographic features and not for prominent topographic features found in the Indonesian Seas.

Since the area of concern is near the equator so that $f \cong 0$, and N is much larger than the semidiurnal and/or diurnal tidal frequencies, the vertical energy flux (7) can be simplified to

$$F_z' \cong \frac{\rho_0 N}{k} w^2 \quad (8)$$

Equation (8) provides rough estimates of baroclinic energy conversion when it is

evaluated at the ocean bottom. w at the ocean bottom is approximately given by

$$w = u\frac{\partial h}{\partial x} + v\frac{\partial h}{\partial y} \qquad (9)$$

The drag stress term parameterizing the baroclinic energy conversion is then given by

$$\tau_x = \frac{1}{k} N_b w^2 \frac{u}{u^2 + v^2} \qquad (10)$$

$$\tau_y = \frac{1}{k} N_b w^2 \frac{v}{u^2 + v^2} \qquad (11)$$

where N_b is the buoyancy frequency at the ocean bottom which is calculated from a climatology of salinity [*Levitus et al.*, 1994] and temperature [*Levitus and Boyer*, 1994]. Equations (10) and (11) are incorporated into the momentum equations (2) and (3).

Following *Jayne and St. Laurent* [2001] and *Tanaka et al.* [2007], horizontal wave number k is regarded here as a tuning parameter to find the most accurate tidal elevation field in the Indonesian Seas. It is also expected for the parameter k to compensate possible errors brought by several ambiguous assumptions in this parameterization such as somewhat crude incorporation of bottom boundary condition.

Figures 6, 7 and 8 show the result of numerical experiment where the drag stress terms with the optimal value of k=2π/(100 km) are incorporated into momentum equations. We find that the RMS difference averaged in the Indonesian Seas for numerical experiment with parameterization can be reduced down to 6.30 cm, which is about half of the RMS difference for numerical experiment without parameterization (11.18 cm).

The results for the other three major tidal constituents (S_2, K_1, O_1) are summarized in Table 1. We can see that after incorporating the parameterization (10) and (11), the spatially averaged RMS difference is reduced by a factor of two for each tidal constituent.

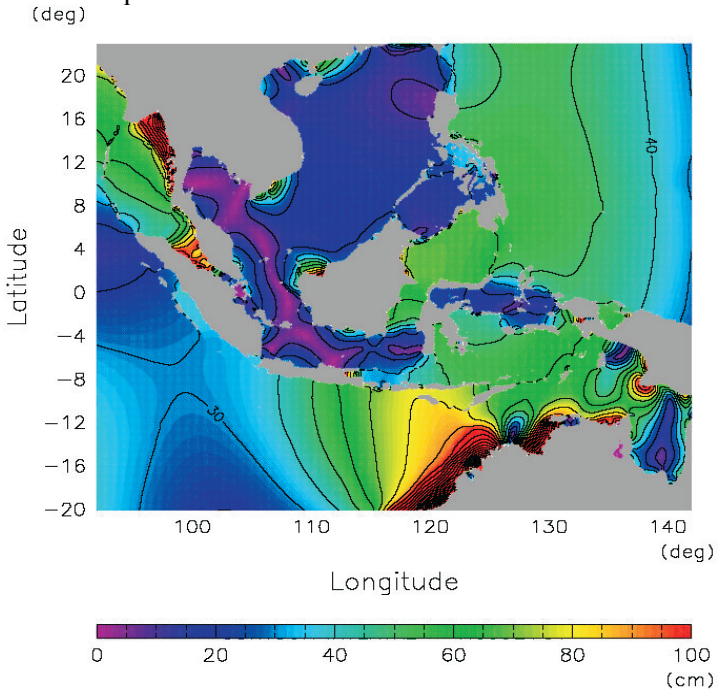

Figure 6. As in Figure 2, but for the result of numerical experiment including parameterization.

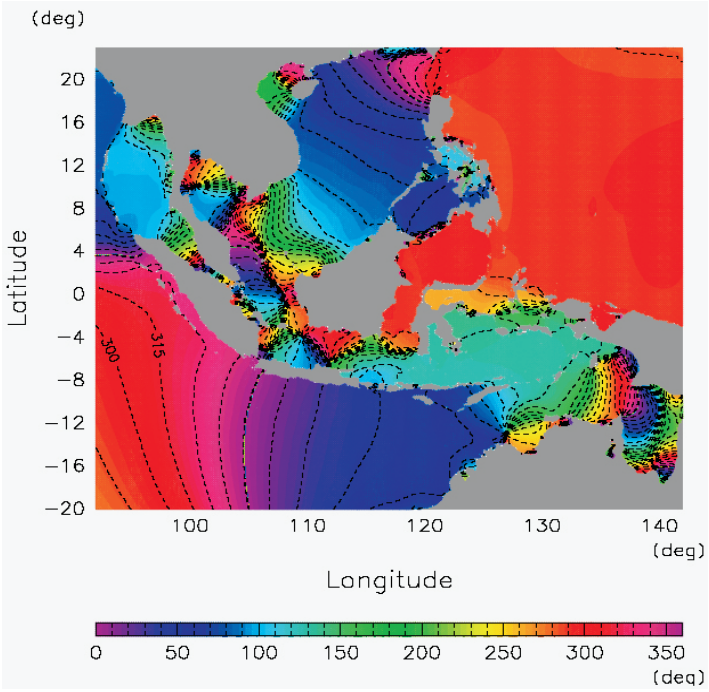

Figure 7. As in Figure 3, but for the result of numerical experiment including parameterization.

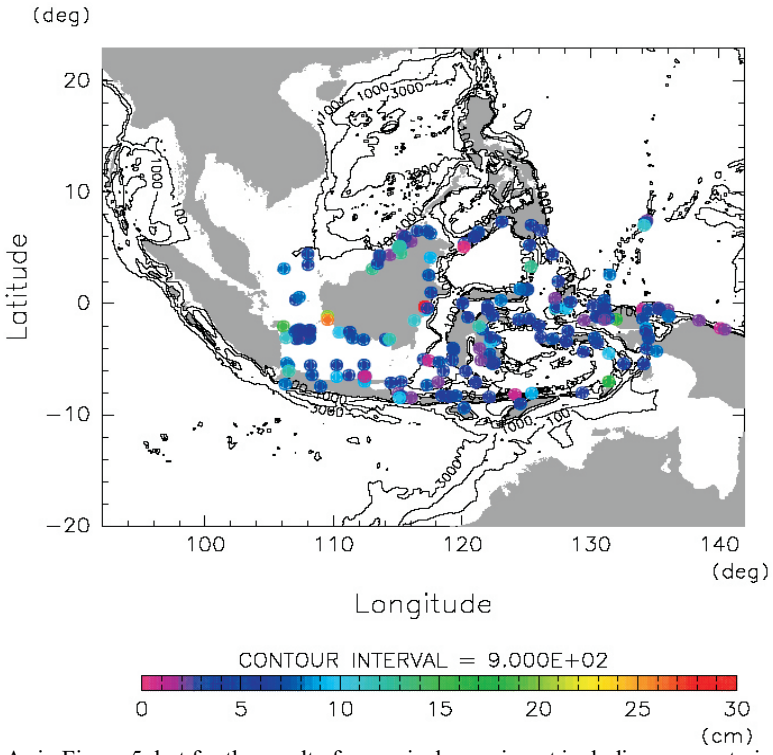

Figure 8. As in Figure 5, but for the result of numerical experiment including parameterization.

Tabel 1. Averaged RMS difference between the model-predicted tidal elevations and observed data with and without parameterization, the value of the tuning parameter *k* which gives the most accurate tidal elevations in the Indonesian Seas for the major four tidal constituents (M_2, S_2, K_1, O_1)

	M_2	S_2	K_1	O_1
Without parameterization, cm	11.18	7.62	12.06	10.44
With parameterization, cm	6.30	3.96	8.48	5.84
Value of $2\pi/k$, km	100	100	100	100

5. Estimates of Energy Lost by the Barotropic Tides to Internal Waves

On the basis of the calculated result in the previous section, we can estimate the energy lost by the barotropic tides to internal waves in the Indonesian Seas. Equations (1) - (3) can be combined into a single energy conservation equation given by

$$\frac{\partial}{\partial t}\left[\frac{1}{2}\rho_0(u^2+v^2)D \quad \frac{1}{2}\rho_0 g\eta^2\right] = \tag{12}$$
$$-\nabla.(\rho_0 gD\vec{u}\eta) - \nabla\left[\frac{1}{2}\rho_0(u^2+v^2)\vec{u}D\right] + \rho_0 gD\vec{u}.\nabla(\beta\zeta)$$
$$+\rho_0 gD\vec{u}.\nabla\eta_{SAL} - \rho_0 C_d|\vec{u}|^3 \quad \rho_0\frac{1}{k}N_b w^2 - Dis_H$$

where Dis_H denotes the energy dissipation associated with the horizontal viscosity.

Figure 9 shows the spatial distribution of the sixth term on the right-hand side of equation (12) which represents the energy conversion from barotropic tides to internal waves. We can see that a large amount of energy is fed into internal waves in the Indonesian Seas especially over the ITF region with a series of large, deep, semi enclosed-basins connected via narrow straits. Three main regions of large energy conversion in the ITF routes can be distinguished on the map. The energy conversion for entrance routes of ITF is represented by energy distributions in the eastern (A) and western (B) areas. Exit routes are represented by southern area (C). Table 2 shows the estimates of each term in equation (12) integrated within the white rectangles in Figure 9. We can see that energy conversion from barotropic tides to internal waves reaches ~51.9 GW in the eastern area (Halmahera, Seram, Banda and Maluku Seas), ~7.5 GW in the western area (Makassar and Flores Seas), and ~26.7 GW in the southern area (Lombok Strait and Timor Passage). The spatial distribution of energy conversion in the entrance and exit routes of ITF is therefore highly heterogeneous. The results show A. B and C areas are "hot-spot" for internal waves generation with clear differences with other parts in the Indonesian Seas.

The results for the other three major tidal constituents (S_2, K_1, O_1) are summarized in Table 3. The total energy conversion from barotropic tides to internal waves in the whole Indonesian Seas reaches ~134.6 GW.

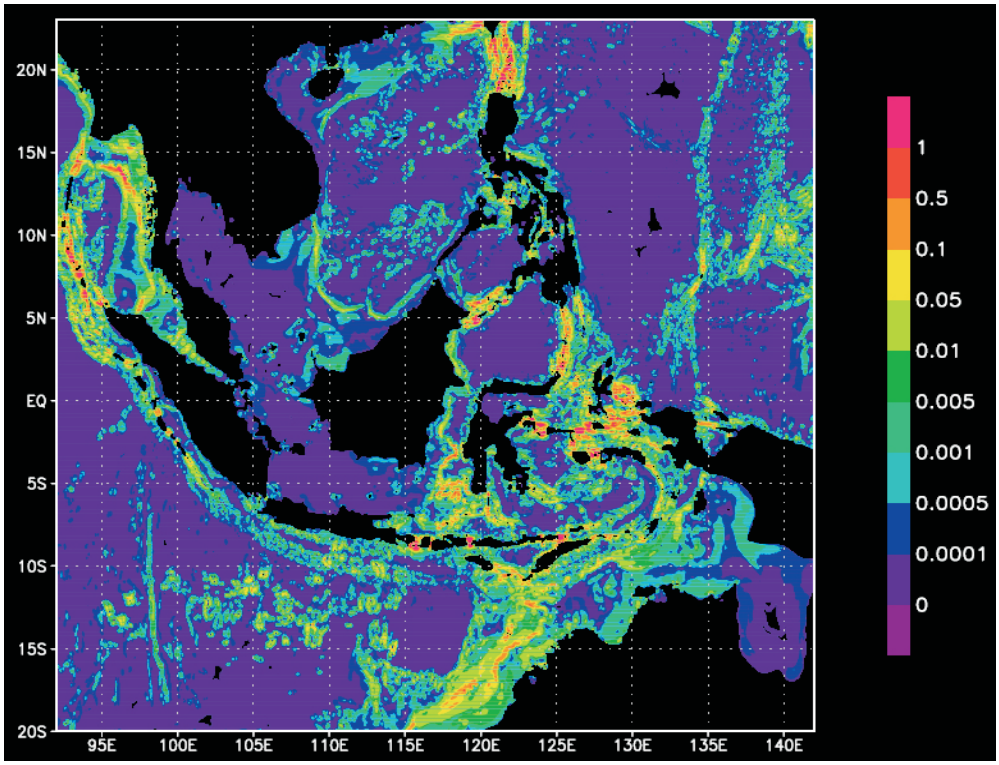

Figure 9. Model predicted distribution of the energy conversion rate from the barotropic tides to internal waves. The energy balance shown in Table 2 is examined within the white rectangles.

Tabel 2. Energy balance (GW) within the white rectangles in the Indonesian Seas [a]

Parameter	Halmahera, Seram, Maluku and Banda Seas (A)	Makasssar and Flores Seas (B)	Lombok Strait and Timor Passages (C)
Net energy flux into domain	**-51.0**	**-7.2**	**-27.0**
Work done by tidal forcing	**1.9**	**-0.3**	**2.2**
Work done by the solid earth	**-5.1**	**-0.8**	**-3.6**
Energy dissipation rate due to bottom friction	**1.9**	**0.7**	**2.4**
Energy dissipation rate due to horizontal viscosity	**0.1**	**0.0**	**0.3**
Energy dissipation rate due to internal wave generation	**51.9**	**7.5**	**26.7**

[a]See Figure 9.

Tabel 3. Estimates for the energy conversion from the barotropic tides to internal waves in the Indonesian Seas for the major four tidal constituents (M_2, S_2, K_1, O_1)

Energy conversion to internal wave (GW)	Semi diurnal		Diurnal	
	M2	S2	K1	O1
Halmahera, Maluku, Seram and Banda Seas (A)	51.9	10.3	17.4	7.8
Makasar and Flores Seas (B)	7.5	2.5	1.0	0.5
Lombok Strait and Timor Passages (C)	26.7	6.6	1.6	0.8
Total	86.1	19.4	20.0	9.1

6. Estimates of Diapycnal Diffusivity in the Indonesian Seas

Turbulent dissipation rate ε (W kg^{-1}) is related to the convergence of upward energy flux of internal waves emanating from the bottom topography. In the present study, the expression of ε follows *St. Laurent et al.* [2002] and *Tanaka et al.* [2007] such that

$$\varepsilon = \frac{q}{p} E(x,y) F(z) \qquad (13)$$

where E(x,y) (W m^{-2}) is the baroclinic energy conversion, q is the local dissipation efficiency, namely, the fraction of energy likely to dissipate locally by turbulent processes, and F(z) (m^{-1}) represents the depth dependence of dissipation rates satisfying

$$\int_{-H}^{0} F(z)\, dz = 1 \qquad (14)$$

Following *St. Laurent et al.* [2002] and *Tanaka et al.* [2007], we assume

$$F(z) \quad \frac{\exp\left[-(H+z)/\zeta\right]}{\zeta\left[1-\exp(-H/\zeta)\right]}, \qquad (15)$$

with ζ=500 m. Although q=0.3 is suggested as an upper bound "local dissipation efficiency" for the semidiurnal internal tides [*St. Laurent and Garrett,* 2002; *Klymak et al.,* 2006; *Legg and Huijts,* 2006], there is no definite general information on the value of q. Bearing in mind that there must be large uncertainty of the value of q, we employ here a crude assumption of q=0.3 for both the semidiurnal and diurnal internal tides.

The diapycnal diffusivity is estimated following *Osborn* [1980], namely,

$$K\rho = \frac{\gamma\varepsilon}{N^2} \quad \frac{\gamma q E(x,y) F(z)}{\rho N^2} \qquad (16)$$

where γ is the mixing efficiency assumed to be 0.2 [*Osborn,* 1980]. Figure 10 shows the distribution of diapycnal diffusivity K_ρ vertically averaged throughout the water column. As in Figure 9, three main regions of high diapycnal diffusivity value can be distinguished. We can see that the distribution of K_ρ is close to the distribution of energy conversion on the Figure 9.

Although significant diapycnal mixing with $K\rho > 100 \times 10^{-4}$ m^{2}s^{-1} can be found in the Indonesian Seas, such "mixing hot spots" are much limited. The value of $K\rho$ averaged within the eastern area (Halmahera, Seram, Banda and Maluku Seas), the western area (Makassar and Flores Seas), and the southern area (Lombok Strait and Timor Passage) are estimated to be ~23×10^{-4} m^{2}s^{-1}, ~5×10^{-4} m^{2}s^{-1}, and ~10×10^{-4} m^{2}s^{-1}, respectively.

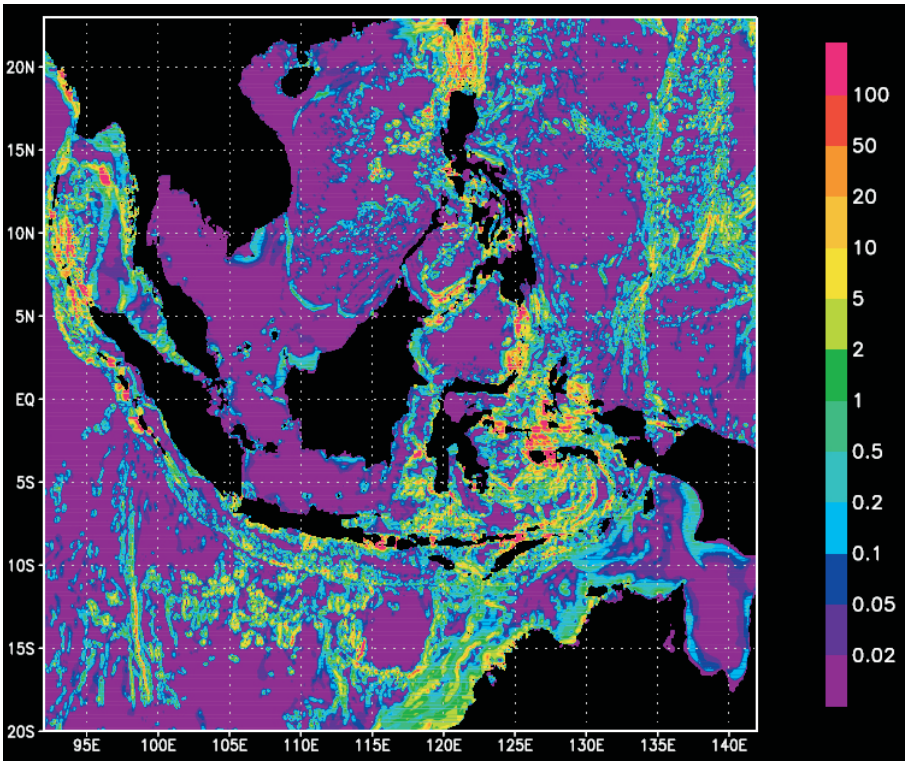

Figure 10. Distribution of diapycnal diffusivity vertically averaged throughout the water column.

7. Summary and Discussion

In the present study, quantitative estimates of diapycnal diffusivity in the Indonesian Seas have been carried out. For this purpose, we have paid attention to the result of numerical experiment that, to reproduce realistic tidal elevation field in the Indonesian Seas and surrounding regions, the energy lost by the incoming barotropic tides to internal waves within the Indonesian Seas should be taken into account.

We have parameterized this baroclinic energy conversion in terms of drag stress terms which are incorporated into the momentum equations. It has been shown that the model predicted tidal elevations in the Indonesian Seas best fit the observed data when we take into account the baroclinic energy conversion in the Indonesian Seas ~86.1 GW for the M_2 tidal constituent and ~134.6 GW for the major four tidal constituents (M_2, S_2, K_1, O_1).

On the basis of this energy conversion, we have estimated diapycnal diffusivity. It has been shown that the value of K_ρ vary from a few 10^{-4} m^2s^{-1} to a hundreds of 10^{-4} m^2s^{-1}. The averaged value of $K\rho$ becomes ~23 × 10^{-4} m^2s^{-1} for the eastern area (Halmahera, Seram, Banda and Maluku Seas), ~5 × 10^{-4} m^2s^{-1} for the western area (Makasar and Flores Seas), and ~10× 10^{-4} m^2s^{-1} for the southern area (Lombok Strait and Timor Passage), respectively.

There are some limitations with the numerical approach in the present study. Most serious one may be found in the oversimplified parameterization for the baroclinic energy conversion. For more accurate estimates of diapycnal diffusivity in the Indonesian Seas, a sophisticated parameterization better suited for prominent topographic features is

necessary. We also need more accurate information about the local dissipation efficiency q. In order to reproduce more realistic tidal elevation field in the Indonesian Seas, we might also need more accurate bathymetry data and high resolution numerical experiment [*Koropitan* and *Ikeda*, 2008].

Not only the averaged value but also the spatial distributions of $K\rho$ revealed in the present study are very different from those assumed in the previous ocean general circulation models [*Schiller et al.,* 1998]. Diapycnal mixing in the Indonesian Seas is known to have great impacts on large scale circulation and water mass properties not only in the Indonesian Seas but also in the Indian Ocean. We believe that the spatial distribution of $K\rho$ revealed here, therefore, must be taken into account in the future numerical models in order to better understand the global ocean circulation.

Acknowledgement

The authors express their gratitude to K. Matsumoto and T. Hibiya for kindly providing Tidal Harmonic data. The author also likes to thank BPKLN under Ministry of National Education for funding scholarship to the author. This work is a collaborative work between Chiba University, University of Tokyo and Udayana University.

References

Egbert, G. D., and R. D. Ray (2001), Estimates of M_2 tidal energy dissipation from Topex/Poseidon altimeter data, *J. Geophys. Res.*, *106*, 22,475-22,502.

Ffield, A., and A. L. Gordon (1992), Vertical mixing in the Indonesian thermocline, *J. Phys. Oceanogr.*, *22*, 184-195.

Ffield, A., and A. L. Gordon (1996), Tidal mixing signatures in the Indonesian Seas, *J. Phys. Oceanogr.*, *26*, 1,924-1,937.

Gill, A. E. (1982), *Atmosphere-Ocean Dynamics,* 662 pp., Academic Press, San Diego, Calif.

Gordon, A. (1986), Interocean exchange of thermohaline water, *J. Geophys. Res.*, *91*, 5037-5046.

Gordon, A. L., A. Ffield and A. G. Ilahude (1994), Thermocline of the Flores and Banda Seas, *J. Geophys. Res.*, *99*, 18,235-18,242.

Hatayama, T., T. Awaji, and K. Akitomo (1996), Tidal currents in the Indonesian Seas and their effect on transfort and mixing, *J. Geophys. Res.*, *101*, 12,353-12,373.

Hatayama, T. (2004), Transformation of the Indonesian Throughflow water by vertical mixing and its relation to tidally generated internal waves, *J. Oceanogr.*, *60*, 569-585.

Hirst, A. C., and J. S. Godfrey (1993), The role of Indonesian Throughflow in a global ocean GCM, *J. Phys. Oceanogr.*, *23*, 1057-1086.

Jayne, S. R., and L. C. St. Laurent (2001), Parameterizing tidal dissipation over rough topography, *Geophys. Res. Lett.*, *28*, 811-814.

Kantha, L. H. (1995), Barotropic tides in the global oceans from a nonlinear tidal model assimilating altimetric tides: 1. Model description and results, *J. Geophys. Res., 100*, 25,283 – 25,308.

Klymak, J. M., J. N. Moum, J. D. Nash, E. Kunze, J. B. Girton, G. S. Carter, C. M. Lee, T. B. Sanford, and M. C. Gregg (2006), An estimate of tidal energy lost to turbulence at the Hawaiian Ridge, *J. Phys. Oceanogr.*, *36*, 1148-1164.

Koropitan, A. F, and M. Ikeda (2008), Three-dimensional modeling of tidal circulation and mixing over the Java Sea, *J. Oceanogr.* , *64*, 61-80.

Larrouy, A. K., G. Madec, P. B. Aubertot, T. Gerkema, L. Bessieres, and R. Molcard (2007), On the transformation of Pacific Water into Indonesian Throughflow Water by internal tidal mixing, *Geophys. Res. Lett., 34,* L04604, doi: 10.1029/2006GL028045.

Legg, S., and K. M. H. Huijts (2006), Preliminary simulations of internal waves and mixing generated by finite amplitude tidal flow over isolated topography, *Deep Sea Res., Part II, 53*, 140-156.

Levitus, S., and T. P. Boyer (1994), *World Ocean Atlas 1994,* vol. 4, *Temperature, NOAA Atlas NESDIS,* vol. 4, NOAA, Silver Spring, Md.

Levitus, S., R. Burgett, and T. P. Boyer (1994), *World Ocean Atlas 1994,* vol. 3, *Salinity, NOAA Atlas NESDIS,* vol. 4, NOAA, Silver Spring, Md.

Matsumoto, K., T. Takanezawa, and M. Ooe (2000), Ocean tide models developed by assimilating TOPEX/POSEIDON altimeter data into hydro dynamical model: A global model and regional model around Japan, *J. Oceanogr.*, *56*, 567 – 581.

Miyama, T., T. Awaji, K. Akitomo, and N. Imasato (1995), Study of seasonal transport variations in the Indonesian Seas, *J. Geophys. Res.*, *100*, 20,517-20,541.

Niwa, Y., and T. Hibiya (2001), Numerical study of the spatial distribution of the M_2 internal tide in the Pacific Ocean, *J. Geophys. Res., 106,* 22,441-22,449.

Osborn, T. R. (1980), Estimates of the local rate of vertical diffusion from dissipation measurements, *J. Phys. Oceanogr.*, *10*, 83-89.

Polzin, K. L., J. M. Toole, J. R. Ledwell, and R. W. Schmitt (1997), Spatial variability of turbulent mixing in the abyssal ocean, *Science.*, *276*, 93-96.

Ray, R. D., G. D. Egbert and S. Y. Erofeeva (2005), A brief overview of tides in the Indonesian Seas, *Oceanography.*, *18*, 74-79.

Schiller, A., J. S. Godfrey, P. C. McIntosh, and G. Meyers, S. E. Wijffels (1998), Seasonal near-surface dynamics and thermodynamics of the Indian Ocean and Indonesian Throughflow in a global ocean general circulation model, *J. Phys. Oceanogr.*, *28*, 2288-2312 .

Simmons, H. L., R. W. Hallberg, and B. K. Arbic (2004), Internal wave generation in a global baroclinic tide model, *Deep Sea. Res.*, *51*, 3043-3068.

Smagorinsky, J. S. (1963), General circulations experiments with the primitive equations, I, The basic experiment, *Mon. Weather Rev.*, *91*, 99-164.

St. Laurent, L. C., and C. Garrett (2002), The role of internal tides in mixing deep ocean, *J. Phys. Oceanogr.*, *32*, 2882-2899.

St. Laurent, L. C., H. L. Simmons, and S. R. Jayne (2002), Estimating tidally driven mixing in the deep ocean, *Geophys. Res. Lett.*, *29*, 2106, doi:10.1029/2002GL015633.

Tanaka, Y., T. Hibiya, and Y. Niwa (2007), Estimates of tidal energy dissipation and diapycnal diffusivity in the Kuril Straits using TOPEX/POSEIDON altimeter data, *J. Geophys. Res.*, *112*, C10021, doi: 10.1029/2007JC004172.

Appendix: Observed data obtained from international tides gauges record in the surrounding Indonesian Seas

No	Longitude	Latitude	Station	Amplitude (m)				Phase (deg)			
	E	N(+) / S(-		M2	S2	K1	O1	M2	S2	K1	O1
1	113.59	4.23	Miri	0.16	0.08	0.36	0.31	341.9	22	323.3	270.6
2	121	6.04	Jolo	0.17	0.11	0.26	0.25	226.6	272.3	315.1	274.9
3	115.04	5.02	Muara Harbour	0.31	0.15	0.4	0.36	346	25	329	271
4	115.24	4.51	Pasar Lawas	0.31	0.14	0.47	0.41	339	29	313	264
5	114.39	4.37	Seria	0.21	0.08	0.35	0.31	300	1	313	265
6	125.38	7.05	Davao	0.59	0.3	0.15	0.02	155.4	197.1	237.5	207.6
7	131.49	2.59	Heren Syo	0.49	0.23	0.19	0.16	203.2	229.4	212.6	194.7
8	121.58	-2.32	Boengkoe	0.44	0.18	0.27	0.18	359.9	67.1	293.4	258.6
9	122.55	-3.28	Poeloe Kokoila	0.54	0.17	0.28	0.19	20	84.2	304.4	291.6
10	122.51	-5.31	Wadjo B	0.49	0.15	0.31	0.17	9.2	89.3	304.5	276.7
11	122.37	-5.28	Boeton	0.53	0.16	0.31	0.2	6.6	70.8	310.7	280.9
12	122.38	-5.42	Bola (Boeton)	0.5	0.14	0.27	0.21	7.6	55.7	305.7	281.9
13	107.06	0.35	Tebon Islet	0.05	0.03	0.28	0.27	175.7	127.8	114.2	30.5
14	107.34	0.59	Tambelan B	0.09	0.04	0.2	0.23	101.8	149.9	92.7	24
15	122.16	-4.53	Poloe Galia	0.68	0.23	0.35	0.2	11.3	74.5	303.1	280.3
16	122.18	-5.13	Tampona Who	0.57	0.17	0.33	0.21	8.3	63.4	303	279.2
17	121.48	-5.1	Poeloe Baleara	0.56	0.18	0.37	0.19	358.3	57.4	292.5	275.7
18	120.28	-6.07	Benteng	0.39	0.1	0.32	0.21	354.9	66.1	299.9	272.1
19	114.47	-7.1	Poeloe Telangoe	0.25	0.15	0.4	0.22	320.8	324.4	300	264.8
20	115.27	-7	Saoebi, Kangean	0.26	0.14	0.27	0.17	317.5	342.8	298.4	270.1
21	115.05	-8.06	Buleleng, Bali	0.29	0.15	0.31	0.21	321.2	342.8	308.7	256.5
22	115.3	-8.32	Teluk Padang	0.34	0.17	0.32	0.17	301.4	337	296.3	262.1
23	115.3	-8.41	Sanur, Bali	0.57	0.14	0.38	0.2	276.4	333	321.3	256.1
24	121.06	-7.07	Kg. Bone Rate	0.45	0.11	0.31	0.19	0.7	56.8	294.2	281.4
25	109	-7.44	Cilacap	0.5	0.25	0.19	0.12	248.4	318	282.8	263.6
26	106.24	-7.24	Genteng B	0.37	0.19	0.12	0.07	234.6	307.2	256.4	240.2
27	106.36	-5.35	Duizend E.	0.01	0.05	0.28	0.07	270.2	22.8	171.2	136
28	112.38	-5.5	Sangkapura B	0.04	0.05	0.43	0.25	64.1	15.7	326.2	291.9
29	112.34	-6.54	Ujung Pangka	0.03	0.06	0.51	0.24	125.2	11.9	326.2	271
30	112.48	-6.54	Tanjung Modeng	0.02	0.06	0.52	0.24	95.8	8.4	326	253.8
31	112.44	-6.56	Karang Jamuang	0.04	0.08	0.54	0.26	16	356	317	259
32	112.41	-7-.02	Sembilangan	0.18	0.16	0.46	0.25	348	3.6	319.1	268.9
33	116.03	-8.43	Labuan Tring B	0.27	0.16	0.35	0.23	308.3	316.9	283.8	264.5
34	117.27	-7.32	Poeloe Sailoes	0.3	0.11	0.33	0.26	6	67.1	294.9	274.1
35	118.13	-7.04	Poeloe Sapoeka	0.34	0.1	0.35	0.2	359.4	343.6	301.1	282.3
36	118.43	-8.27	Bima	0.35	0.1	0.3	0.1	3.4	54.6	303.6	255.8
37	119.02	-8.34	Safe B. Sumbawa	0.49	0.18	0.2	0.2	347.8	37.9	288.3	269.5
38	119.53	-8.29	Labuan Badjo	0.46	0.16	0.27	0.17	343.1	39.2	288.4	284.7

No	Longitude	Latitude	Station	Amplitude (m)				Phase (deg)			
	E	N(+) / S(-)		M2	S2	K1	O1	M2	S2	K1	O1
39	122.13	-8.39	Maoemere	0.53	0.16	0.3	0.24	2.4	61.6	301.1	275.3
40	120.15	-9.38	Nangamessi B.	0.83	0.41	0.26	0.16	298.4	349.5	287.1	275.3
41	131.06	0.3	Ajoe, New Guine	0.55	0.19	0.1	0.14	181.7	235.8	214.3	197.4
42	134.32	-2.22	Jende, New G.	0.57	0.23	0.21	0.14	209.8	223.9	201.8	189
43	134.53	-3.12	Kwatisore Bay	0.61	0.21	0.2	0.13	199.1	237.2	214.5	188.6
44	134.5	-3	Moor Islets	0.54	0.24	0.21	0.14	209.2	240.3	213.5	184.7
45	124.13	-8.16	Kabir, Pantar I.	0.53	0.21	0.25	0.24	357.4	64.6	298.1	264.3
46	124.53	-9.01	Atapoepoe	0.56	0.31	0.21	0.15	318.1	14.2	298.4	261.7
47	129.5	-1.5	Waigama	0.18	0.19	0.17	0.1	98.2	181.3	299.5	269.7
48	127.26	-0.41	Laboeha	0.09	0.1	0.21	0.08	54.5	174.1	273.4	215.1
49	127.36	-0.3	Sabatang	0.22	0.17	0.19	0.15	146.2	198.8	268.2	240.9
50	128.12	-0.42	Cane B.	0.16	0.14	0.2	0.1	100	161.6	277.6	270.3
51	127.22	0.47	Ternate Island	0.27	0.22	0.14	0.1	160.6	197.3	261.5	240.1
52	127.48	2	Asimiro	0.4	0.18	0.16	0.12	175.8	223.4	235	206.7
53	128.45	0.15	Patani	0.14	0.15	0.14	0.1	133.9	187.5	265.1	206.8
54	131.06	-1	Samate	0.42	0.18	0.23	0.12	190.7	233.8	208.3	195.4
55	131.13	-0.5	Sorong	0.41	0.18	0.23	0.13	194.4	209.6	226.2	171.3
56	131.01	-0.54	Poeloe Jef Doif	0.44	0.17	0.16	0.1	199.8	241	210.4	206.5
57	130.2	-0.21	Moetoes Besar	0.28	0.19	0.17	0.1	170.2	217.3	263	253.2
58	127.06	-3.16	Kajeli Bay	0.34	0.12	0.2	0.11	15.2	111.8	306.7	270.4
59	126.13	-3	Bara Bay	0.4	0.13	0.33	0.17	20.9	100.6	309.6	286.3
60	126	-2	Sanana	0.28	0.12	0.31	0.21	49.4	145	298.8	269.5
61	124.42	-1.42	Gela	0.13	0.19	0.17	0.09	123	218.6	272.1	231.8
62	125.24	-1.36	Dofa	0.18	0.18	0.24	0.16	116.6	197.2	272.4	233.1
63	125.12	1.27	Kg. Aer Tembaga	0.36	0.26	0.26	0.13	146	191	258	226
64	134.3	-2.44	Wassior	0.61	0.24	0.22	0.16	209	256	223	196
65	121.28	6.44	Dassalan Island	0.2	0.12	0.27	0.22	242.9	280.1	306.9	265.1
66	120.17	5.39	North Lahatlahat	0.13	0.09	0.23	0.22	229.3	267.4	303	266.3
67	123.1	7.35	Margosatubig	0.62	0.37	0.14	0.12	162.5	206.7	258.2	238.4
68	125.26	5.25	Lajan Point	0.57	0.31	0.18	0.12	160	200.1	249.	218.1
69	126.13	6.57	Pujada Bay	0.55	0.24	0.17	0.13	158.4	191.6	207.1	182.3
70	107.33	-3.12	Selioe Island	0.09	0.06	0.51	0.34	29	21	142	92
71	108.05	-3.14	Tg. Batoe Hitam	0.09	0.01	0.38	0.23	346	76	137	68
72	108.16	-3.04	Ajam Besar	0.08	0.01	0.4	0.24	351	76	136	87
73	113.02	3.11	Kwala Bintulu	0.16	0.06	0.47	0.32	44	32	320	271
74	117.19	-0.59	Kutei River	0.51	0.4	0.21	0.15	133	193	271	248
75	115.36	6.12	Palau Mangalum	0.24	0.1	0.34	0.31	320	358	312	275
76	119.36	-4.13	Tg. Lasonraai	0.13	0.22	0.25	0.2	128	220	297	267
77	106.15	3.14	Salat Peninting	0.19	0.06	0.39	0.29	240	285	359	315
78	117.55	6.3	Lankayan Island	0.33	0.18	0.33	0.3	310	347	322	278

No	Longitude	Latitude	Station	Amplitude (m)				Phase (deg)			
	E	N(+) / S(-)		M2	S2	K1	O1	M2	S2	K1	O1
79	117.29	6.53	Tigabu Island	0.33	0.18	0.37	0.31	312	353	320	280
80	115.54	5.45	Kuala Papar	0.21	0.1	0.35	0.3	308	352	312	261
81	115.4	5.42	Pulau Tega	0.26	0.11	0.36	0.31	317	0	315	254
82	107.15	-2.39	Akbar Droogte	0.05	0.06	0.53	0.48	129	79	159	107
83	107.3	-3	Poeloe Roe	0.05	0.06	0.57	0.32	61	79	146	90
84	125.37	3.31	Menaloe, Sangi I.	0.54	0.37	0.22	0.12	149.6	199.8	247.7	226.9
85	134.36	-4.04	Poeloe Lakahita	0.62	0.18	0.28	0.19	42	114	342	329
86	136.12	-1.11	Bosnik, Biak	0.45	0.17	0.25	0.15	193.5	230.6	216.2	179.3
87	136.02	-0.55	Korim, Biak	0.42	0.12	0.19	0.15	188.8	228.9	208.3	185.5
88	135.3	-0.38	Mios Woendi	0.44	0.19	0.25	0.14	189.9	220	224.9	188
89	140.1	-2.21	Demta Bay	0.32	0.08	0.25	0.15	192.5	232.7	207.2	181.3
90	106.5	-5.57	Edam	0.05	0.07	0.27	0.08	312.2	334.3	154.5	133.7
91	108.21	-5.55	Boompjes Island	0.11	0.06	0.14	0.07	339.2	241.3	114	121.2
92	108.34	-6.42	Cheribon	0.16	0.1	0.14	0.05	332.7	206.9	63.8	169
93	110.25	-5.53	Karimoen Djawa	0.02	0.05	0.23	0.04	257	3.2	6.9	263.1
94	110.25	-6.58	Semarang	0.1	0.08	0.22	0.08	286	187.2	8.9	246.1
95	111.2	-6.43	Rembang	0.04	0.02	0.41	0.15	7.2	337.3	352	256.2
96	106.11	-2.05	Pangkal Pinang	0.06	0.02	0.72	0.54	172.5	327.6	142.1	74.4
97	107.13	-3.19	Ondiepwater	0.08	0.07	0.53	0.28	83.4	67.6	159.1	103.3
98	107.37	-2.32	Poeloe Langkoeas	0.02	0.03	0.64	0.38	253.6	40.8	153.7	89.9
99	108.18	-2.36	Manggar	0.02	0.06	0.41	0.27	18.3	351.4	152	108.2
100	108.1	-2.58	Gantoeng	0.07	0.04	0.39	0.23	20.5	23.7	168.2	116.4
101	115.13	-8.45	Benoa, Bali	0.71	0.33	0.25	0.12	286.4	354.6	301.1	276.3
102	117.12	-0.3	SUngai Mariam	0.57	0.31	0.21	0.16	203.5	258.6	305.1	279.3
103	125.05	1.22	Kema	0.21	0.27	0.17	0.11	142.7	179.8	255.2	238.5
104	123.03	0.3	Gorontalo	0.15	0.21	0.25	0.1	100.8	166.9	281.3	215.5
105	120.06	0.03	Menelili	0.21	0.18	0.22	0.15	116.7	174.8	272.2	221.4
106	120.46	-1.22	Poso	0.23	0.23	0.16	0.12	113.3	164.5	262.6	221.8
107	122.4	-1.09	Kintong	0.3	0.18	0.26	0.18	23.5	108.7	312.7	265.9
108	119.3	-4	Pare Pare Bay	0.12	0.16	0.31	0.15	124.9	207	292.8	253
109	129.35	-8	Tepa	0.57	0.19	0.13	0.12	17.2	86.8	304.3	287.9
110	131.42	-7	Ritabel, Larat I.	0.6	0.17	0.23	0.17	54.5	102.6	331.7	317.8
111	132.58	-5.38	Elat, Kai Island	0.59	0.18	0.24	0.18	39.9	116.1	327.4	311.5
112	134.14	-5.45	Dobo, Aroe I.	0.61	0.19	0.28	0.17	42.4	121.5	326.1	306.3

No	Longitude	Latitude	Station	Amplitude (m)				Phase (deg)			
	E	N(+) / S(-)		M2	S2	K1	O1	M2	S2	K1	O1
109	129.35	-8	Tepa	0.57	0.19	0.13	0.12	17.2	86.8	304.3	287.9
110	131.42	-7	Ritabel, Larat	0.6	0.17	0.23	0.17	54.5	102.6	331.7	317.8
111	132.58	-5.38	Elat, Kai	0.59	0.18	0.24	0.18	39.9	116.1	327.4	311.5
112	134.14	-5.45	Dobo, Aroe I.	0.61	0.19	0.28	0.17	42.4	121.5	326.1	306.3
113	132	-1.42	Waronge	0.69	0.27	0.28	0.22	69.9	160	334.4	295.5
114	131.41	-1.3	Karabra River	0.55	0.26	0.27	0.16	54.5	140.6	321.7	305.8
115	130.46	-1.17	Sailolof	0.25	0.18	0.24	0.15	106.3	186.5	295.6	270.7
116	130.55	-1.24	Peli Islet	0.21	0.2	0.22	0.14	95	173.2	288.5	253.6
117	117.59	1	Benoa Baroe	0.69	0.56	0.22	0.15	160.9	218	275.3	246.6
118	122.2	-3.44	Lembo Badjo	0.48	0.18	0.28	0.17	26.2	109.3	319	265.2
119	115.15	5.16	Labuan	0.27	0.12	0.41	0.33	322.4	8.5	320.1	262.3
120	116.04	5.59	Jesselton	0.24	0.1	0.37	0.31	319	353	315	267
121	116.51	6.53	Kudat	0.29	0.15	0.44	0.25	317	359	313	264
122	117.53	4.14	Tawao	0.76	0.43	0.19	0.22	161	217	260	207
123	114.05	-3.19	Kahajan	0.42	0.06	0.67	0.37	161	89	340	282
124	117.3	-0.42	Beraoe River	0.71	0.39	0.13	0.16	207.4	268	296.3	270.1
125	117.42	2.55	Bulungan R.	0.79	0.51	0.19	0.14	169	216	273	244
126	125.42	-8.05	Liram Island	0.63	0.24	0.31	0.23	30	110	312	298
127	106.31	-3.08	Dapoer Isles	0.17	0.11	0.61	0.32	103.9	78	147.8	95.1
128	108.09	-2.4	Telok Pering	0.02	0.03	0.51	0.37	310.6	293.7	121.1	73.5
129	107.01	-2.52	Tjelaka, Liat I	0.07	0.05	0.67	0.38	81.9	47	142.3	78.6
130	107.38	-2.45	Tanj Pandan	0.08	0.07	0.72	0.42	96	55	154	93
131	122.23	-3.03	Salabangka	0.48	0.19	0.28	0.19	21.1	86.2	303.9	285.2
132	135.35	-0.51	Korido	0.55	0.23	0.24	0.15	194.7	241.8	201.8	186.9
133	121.33	-2.04	Lingkoboe	0.47	0.17	0.3	0.18	351.8	90.9	296.8	245
134	115.58	6.01	Gaya	0.21	0.11	0.3	0.3	311.9	353.1	313.4	262.6
135	121.36	-4.03	Kolaka	0.56	0.16	0.31	0.21	5.7	68.8	291.7	278.9
136	122	-0.56	Tobelombangi	0.19	0.19	0.16	0.14	110	189	274	235
137	127.05	4.43	Karatoeng	0.53	0.26	0.17	0.13	167	195	220	195
138	140.44	-2.33	Hollandia Bay	0.31	0.07	0.22	0.16	195.4	226.5	199.6	179.8
139	120.14	5.08	Gallo Malo C.	0.68	0.38	0.17	0.15	165.4	211.5	263.1	228.3
140	115.08	5	Sapo Point	0.32	0.14	0.41	0.34	334	16	319	266
141	113.42	3.58	Kuala Niah	0.17	0.09	0.37	0.34	347	22	319	266
142	135.15	-4.28	Aidoena	0.49	0.1	0.37	0.33	44	120	24	341
143	114.2	-3.3	Barito River	0.31	0.07	0.64	0.31	135.7	54.3	326.5	248.2
144	114.36	-3.2	Bandjermasin	0.31	0.05	0.59	0.32	175.2	120.8	352.2	290
145	117	-5	Lima Island	0.08	0.09	0.3	0.18	137.4	221	287.8	273.6

No	Longitude	Latitude	Station	Amplitude (m)				Phase (deg)			
	E	N(+) / S(-)		M2	S2	K1	O1	M2	S2	K1	O1
146	131.16	-1.32	Kobalin River	0.51	0.19	0.28	0.18	81	170	326	298
147	136.05	-1.11	Sorido Lago	0.43	0.12	0.2	0.14	219	253	221	192
148	131.08	-1.46	Jef Joes	0.47	0.18	0.28	0.18	74	162	326	301
149	116.29	-1.52	Pasir River	0.64	0.51	0.28	0.18	140	200	281	250
150	109.54	-1.12	Soekadana	0.16	0.13	0.66	0.42	341	353	156	98
151	109.54	-1.46	Pawan River	0.18	0.13	0.5	0.38	324	337	150	94
152	110.44	-2.59	Djelai River	0.12	0.03	0.16	0.1	215.9	157.5	334.1	228.8
153	111.26	-2.54	Waringin R.	0.22	0.06	0.36	0.16	192.5	131.1	333.4	236.1
154	111.48	-3.1	Koemai B.	0.21	0.06	0.33	0.21	172.2	52.9	318.2	268
155	112.34	-3.25	Pemboeang	0.24	0.06	0.41	0.21	172.2	52.9	318.2	268
156	129.43	-4.32	Banda Harbo	0.57	0.22	0.29	0.18	22.9	98.6	312.1	286.8
157	131.42	-4.48	Poeloe Tioor	0.57	0.21	0.32	0.2	31	95.6	314.1	293.8
158	130.54	-3.53	Geser	0.54	0.18	0.28	0.19	23.6	93.2	323.9	285.6
159	130.32	-3.07	Boela B.	0.44	0.15	0.21	0.15	40.3	132.9	301.3	288
160	128.24	-2.48	Taniwel,	0.3	0.14	0.21	0.12	36.6	158.2	307.4	264.1
161	128.11	-3.41	Ambon Bay	0.47	0.17	0.29	0.21	26	93.6	315.7	304.3
162	117.42	-5.12	P. Kalokong	0.08	0.1	0.25	0.17	115.5	207.6	305.6	240.8
163	118.23	-5.25	P. Dewakang	0.11	0.13	0.21	0.14	41.1	190.2	291.9	262.2
164	118.55	-6.05	De Bril Bank	0.21	0.05	0.3	0.18	12	158.2	299.4	268.6
165	119.24	-5.09	Makassar	0.08	0.11	0.28	0.17	63.1	195.2	300.9	270.1
166	108	4.45	Poeloe Laoet	0.09	0.04	0.36	0.18	55.9	56	333.3	268.6
167	108.02	3.48	Sedanau, Nat	0.2	0.07	0.38	0.28	87.8	127.9	340.3	310.6
168	106.52	-6.06	Tanjung Priok	0.05	0.05	0.25	0.13	4.6	311.3	151.9	130.7
169	124.5	1.3	Menado	0.56	0.35	0.16	0.16	158.2	202.3	261.5	220.7
170	122	-0.24	Togian B.	0.23	0.21	0.17	0.14	110.9	173	257.3	230.5
171	113.59	4.35	Kuala Baram	0.17	0.08	0.35	0.3	335	10	319	269
172	121	6.04	Jolo, Jolo	0.17	0.11	0.26	0.25	226.6	272.3	315.1	274.9
173	112.44	-6.56	KarJamuang	0.04	0.08	0.54	0.26	16	356	317	259
174	115.15	5.15	Labua Borneo	0.28	0.13	0.39	0.34	325	357.3	315.3	265.1